PIER M

*(Received 20 August 2024, Accepted 11 October 2024, Scheduled 17 October 2024)*

# A Compact Super-Wideband MIMO Antenna for Wireless Communication Systems

Rania R. Elsharkawy*

*Microstrip Circuits Department, Electronics Research Institute (ERI), Cairo, Egypt*

**ABSTRACT:** This paper presents a super-wideband antenna for operation in X, Ku, K, Ka, V, and W band applications. A monopole antenna with a semi-circular shape, fed through a transmission line and a Co-Planar Waveguide (CPW), is presented. It has a bandwidth ranging from 11.5 GHz to more than 100 GHz. A Multiple-Input Multiple-Output (MIMO) system with quad elements is constructed from the proposed antenna. The MIMO elements are arranged in an orthogonal arrangement to decrease the coupling between them. The MIMO system performance is investigated. The antenna is fabricated and measured, and it has a maximum gain of 8.37 dBi. The maximum radiation efficiency of the proposed antenna reaches 95% over most of the band. For the MIMO system, the maximum Envelope Correlation Coefficient (ECC) is 0.06, and the Diversity Gain (DG) is 9.7 dB.

## 1. INTRODUCTION

The demand for a compact wide-bandwidth antenna is increased. An antenna that operates over a wide bandwidth can accommodate various frequencies without the need for frequent adjustments or tuning. The design of a wide-bandwidth antenna with a low-profile structure is a challenge for researchers. Many researchers have worked on this point. In [1], the authors presented a structure based on an antenna with an H-shaped patch structure, printed on an FR-4 substrate, which is a high-loss substrate. The operating bandwidth of the antenna is from 11.595 GHz to 15.75 GHz. In [2], an antenna with a semi-triangular patch and dimensions of $21 \times 15 \times 3.175\,\text{mm}^3$ is presented. The antenna operating frequency range is from 6 GHz to 21 GHz. The antenna maximum gain is 5.3 dB. Its efficiency is 77%. In [3], the authors presented an antenna with a pentagonal shape. The operating band ranges from 7.6 GHz to 12 GHz. It has a maximum gain of 8.07 dB. In [4], an antenna with inverted triangular patch shape and dimensions of $30 \times 13 \times 0.254\,\text{mm}^3$ is presented. The antenna operating frequency ranges are from 10.87 to 12.76 GHz and 15.19 to 16.02 GHz. It has a gain ranging from 3.34 to 6.08 dBi.

Super-wideband antennas have also been presented by the authors of [5–9]. In [6], the authors present an antenna design printed over an FR4 substrate operating from 1.2 GHz to 40 GHz, with dimensions of $55\,\text{mm} \times 40\,\text{mm} \times 1.6\,\text{mm}$. The authors of [7] present a CPW antenna printed on an FR4 substrate with dimensions of $32\,\text{mm} \times 26\,\text{mm}$, operating from 3.06 GHz to 35 GHz. The authors of [8] present an antenna design with an octagonal radiator and a CPW printed on an FR4 substrate. It works from 3.8 GHz to 68 GHz. In [9], a monopole antenna with a flower shape radiator printed over an FR4 substrate is presented to operate from 3.7 GHz to 60 GHz. In [10], the authors present an antenna with a concentric radiator with semi-elliptical ground plane to operate from 10.3 GHz to 40 GHz.

Due to the advantages of MIMO technology in enhancing the capacity of wireless communication systems in terms of improving the link quality by using multiple antennas to transmit and receive signals, reducing the interference, increasing the Signal-to-Noise Ratio (SNR), increasing the capacity, and increasing the data rate, several researchers have adopted this technology. The authors of [11] present an antenna based on an octagonal shape printed on an FR4 substrate to operate from 3.28 GHz to 17.8 GHz. The achieved peak gain is 4.93 dBi, and the efficiency is 95.34%. Two elements are arranged to establish the MIMO structures with dimensions of $40 \times 23\,\text{mm}^2$. The MIMO system achieves an ECC of 0.003 and a DG of 9.997 dB. In [12], the authors present a four-port MIMO system based on an antenna with COVID-19 shape with dimensions of $50\,\text{mm} \times 50\,\text{mm}$ to cover the frequency range from 2.4 GHz to 18 GHz. It achieves an ECC of 0.00021 and a DG of 9.9 dB. In [13], the authors suggest a tree-shape antenna to operate from 23 GHz to 40 GHz. It has dimensions of $40\,\text{mm} \times 40\,\text{mm}$. A MIMO system with four orthogonal elements is arranged. It has dimensions of $80\,\text{mm} \times 80\,\text{mm}$. The MIMO antenna system achieves a total efficiency of 70%.

In [14], an antenna with three circular rings and a square slot has been presented with a bandwidth from 26.5 GHz to 41 GHz. It has a peak gain of 4 dBi and a radiation efficiency of 96%. An antenna with rectangular and circular patches with two stubs is presented. It works from 26.5 GHz to 43.7 GHz as presented in [15]. Quad elements arranged orthogonally have been used to form the MIMO system. The achieved gain with this structure is 8.4 dBi, and the CCL is 0.001. In [16], the authors present a quad-element with a spade-radiator of a defected ground structure and use a windmill-shape element for the decoupling purpose. They achieve an isolation level of 17 dB,

* Corresponding author: Rania R. Elsharkawy (raniarefaat85@eri.sci.eg).

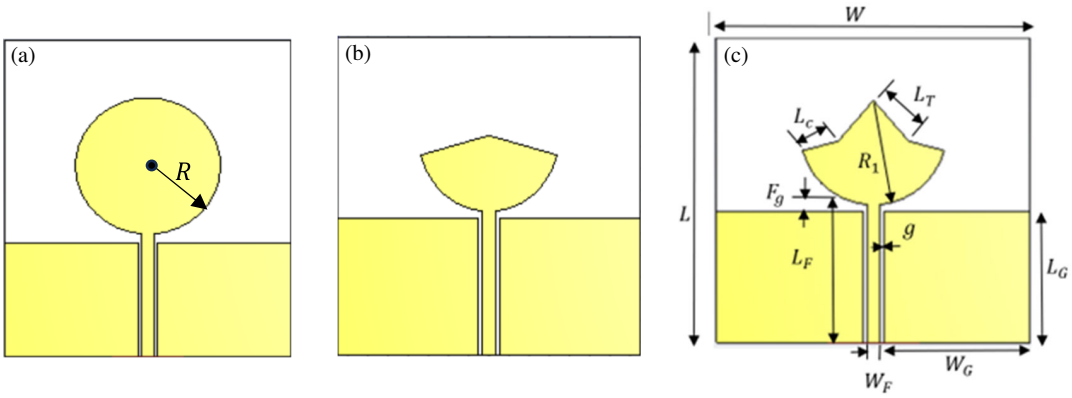


**FIGURE 1**. Design steps. (a) Circular patch antenna. (b) Circular sector patch antenna. (c) Circular sector patch with triangular shape.

which is insignificant. The authors of [17] present a MIMO system with quad elements. It has dimensions of $56 \times 56\,\text{mm}^2$ with an operating bandwidth from 1.3 GHz to 40 GHz and an isolation greater than 22 dB.

The main challenge associated with MIMO systems is the isolation between MIMO system antennas. This isolation affects the quality of the signal and the interference level. It is desirable for the isolation to be maximized, and consequently the coupling between MIMO elements to be minimized, in order to enhance the overall MIMO system performance. Researchers adopted several techniques for reducing the coupling between MIMO antenna elements. A Band-Pass Filter (BPF) has been used to enhance the isolation level by 10 dB [12]. In addition, an array of six electromagnetic band-gap elements was used to enhance the isolation level to 30 dB between two orthogonal MIMO elements [18]. Moreover, a metasurface layer [19] has been adopted for the mutual coupling reduction in MIMO systems.

In this paper, an antenna that operates over a wide bandwidth of 11.5 GHz to more than 100 GHz is presented. It includes a large portion of X band (8 GHz to 12 GHz), Ku band (12.4 GHz to 18 GHz), K band (18 GHz to 27 GHz), Ka band (27 GHz to 40 GHz), V band (40 GHz to 75 GHz), and W band (75 to 110 GHz). The presented work depends on the monopole antenna with a CPW. The parameters of the antenna are optimized through the CST simulator to obtain an antenna design with a good performance regarding the impedance bandwidth, gain, and efficiency. A four-port MIMO system with orthogonal arrangement for the antenna elements is established.

The paper is organized as follows. Section 2 presents the proposed single-element antenna design. Section 3 presents the antenna parametric study. Section 4 introduces the far-field patterns. The proposed quad-port MIMO system is given in Section 5. The MIMO system performance is presented in Section 6. The fabrication and measurements are given in Section 7. Section 8 gives a comparison between the proposed MIMO antenna system and state-of-the-art systems. Finally, Section 9 gives the conclusion.

## 2. ANTENNA DESCRIPTION

The antenna construction begins with a circular patch with radius $R$, calculated according to [20]:

$$R = \frac{A}{\left\{1 + \frac{2h}{\pi\epsilon_r A}\left[\ln\left(\frac{\pi A}{2h}\right) + 1.7726\right]\right\}^{1/2}} \tag{1}$$

$$A = \frac{8.791 \times 10^9}{f_r\sqrt{\epsilon_r}} \tag{2}$$

where $\epsilon_r$ and $h$ are the dielectric constant and height of the substrate material, respectively.

A circular patch antenna is shown in Figure 1(a). The antenna is fed through a CPW with an inset feed. The antenna is printed over a substrate material of Roger's RO3003 type with a dielectric constant $\epsilon_r = 3$, $\tan\delta = 0.001$, and substrate height $h = 0.25$ mm. In the second step, a sectorial shape is cut from the circular patch to produce an antenna with a circular sector patch radiator shape as shown in Figure 1(b). In the third step, a triangular shape is added to produce the antenna's final structure, as shown in Figure 1(c). The benefit of using this shape is to enhance the reflection coefficient values over the band by increasing the surface current distribution over that band. Figure 2 shows a comparison of the reflection coefficient for the three steps of antenna design. From the comparison, we can see that the antenna obtained in the third step introduces a larger bandwidth with the best $S_{11}$ value. The operating bandwidth of the antenna starts from 11.5 GHz to greater than 100 GHz. Figure 3 shows the variation of the real and imaginary parts of the input impedance of the antenna over frequency, which indicates that the imaginary part is around zero and the real part around 50 Ω. In addition, Figure 4 shows the Voltage Standing Wave Ratio (VSWR) over frequency, which ensures that the antenna operating bandwidth is from 11.5 GHz to greater than 100 GHz, since VSWR $< 2$. The antenna surface current distributions at 15 GHz, 30 GHz, 60 GHz, and 80 GHz are shown in Figure 5. The optimum parameters of the designed antenna are shown in Table 1. The best antenna parameters are obtained through an optimization process carried out using the commercial CST package. The main purpose for the optimization process is to get a wide operating bandwidth for the antenna.

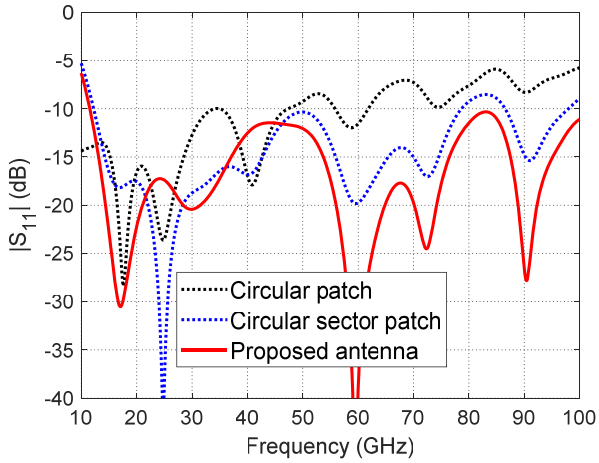


**FIGURE 2**. Comparison between antenna reflection coefficients of the proposed antenna design steps.

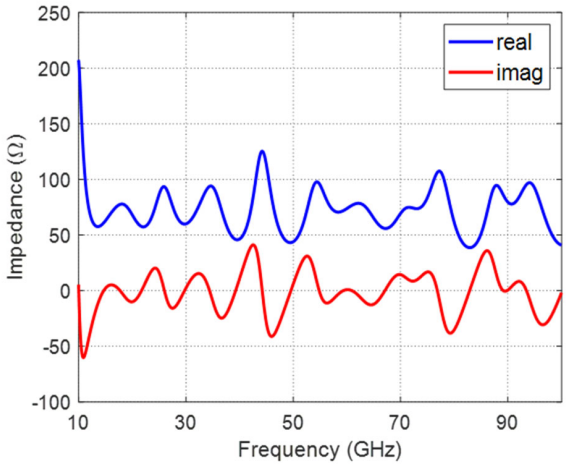


**FIGURE 3**. Real and imaginary parts of the input impedance over the frequency.

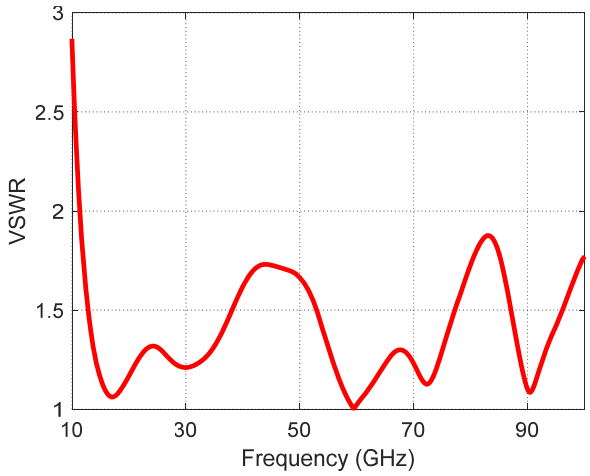


**FIGURE 4**. VSWR over frequency.

**TABLE 1**. Dimensions of the proposed antenna shown in Figure 1.

| Parameter | Value (mm) | Parameter | Value (mm) |
|---|---|---|---|
| $R$ | 3.5 | $L$ | 14.6 |
| $L_F$ | 6.52 | $R_1$ | 5 |
| $W_G$ | 6.98 | $L_G$ | 6.3 |
| $g$ | 0.2 | $F_g$ | 0.37 |
| $W_F$ | 0.63 | $W$ | 15 |
| $L_t$ | 2.58 | $L_C$ | 1.75 |

## 3. ANTENNA PARAMETRIC STUDY

The antenna parameters are studied through an optimization process using the CST simulator to get the best antenna performance. The purpose of this study is enhancing the antenna operating bandwidth through enhancing the $|S_{11}|$ value. Some parameters are selected for this study, including feed line length $(L_F)$, ground plane length $(L_G)$, the gap between the feed line and ground $(g)$, ground plane width $(W_G)$, and the length of the triangular section $(L_T)$. In addition, parameter $L_C$ is considered in the optimization process.

### 3.1. Parametric Study of the Feed Line ($L_F$)

The microstrip feed line has a significant role in enhancing the antenna bandwidth as well as the impedance matching to set the input impedance of the antenna to $50\,\Omega$. The effect of varying $L_F$ on the reflection coefficient magnitude, $|S_{11}|$, is illustrated in Figure 6(a). It is shown that $|S_{11}|$ is varied by varying this parameter. The value of $L_F = 6.52$ mm gives the best bandwidth with the best impedance matching, especially at the upper frequencies of the band.

### 3.2. Parametric Study of the Ground Plane Length ($L_G$)

The ground plane length $(L_G)$ affects the antenna bandwidth and impedance matching. The effect of varying $L_G$ on $|S_{11}|$ is shown in Figure 6(b). It is clear that the value of $L_G = 6.3$ mm gives the widest bandwidth with good impedance matching.

### 3.3. Parametric Study of the Gap between the Feed Line and the Ground (g)

The variation of the gap between the microstrip feed line and the CPW ground plane $(g)$ has a direct effect on the magnitude of the reflection coefficient $|S_{11}|$. Figure 6(c) illustrates this effect. As shown in the figure, the whole-band impedance matching varies with the gap variation. The value of $g = 0.2$ mm is the best choice for achieving a wide bandwidth and impedance matching.

### 3.4. Parametric Study of the Width of the Ground Plane ($W_G$)

The width of each of the two sides of the ground plane $W_G$ has an important role in enhancing the impedance matching and the bandwidth. Figure 6(d) shows the effect of $W_G$ variation on $|S_{11}|$. The value of $W_G = 6.98$ mm gives the best performance.

### 3.5. Parametric Study of the Length of the Triangular Section ($L_T$)

The variation of the triangular length affects the antenna impedance matching. Figure 6(e) shows the variation of $|S_{11}|$

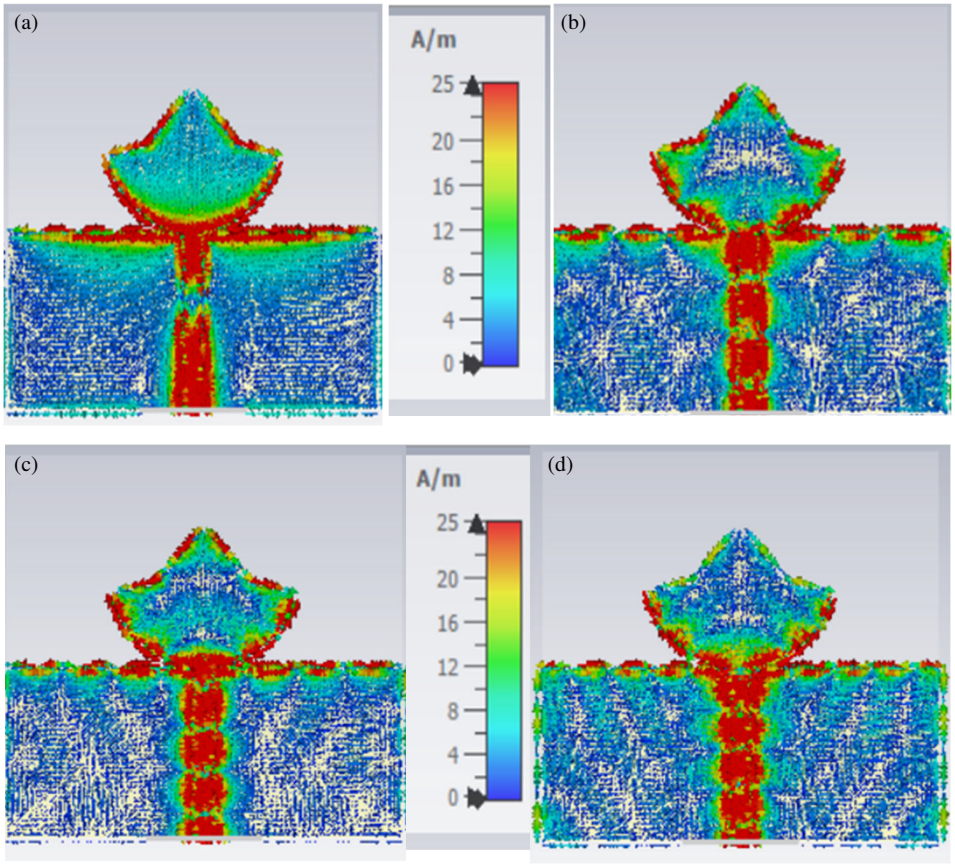


**FIGURE 5**. Surface current density over the antenna at different frequencies (a) 15 GHz, (b) 30 GHz, (c) 60 GHz, and (d) 80 GHz.

over frequencies at different values of $L_T$. The value of $L_T = 3.4$ mm is selected for the final design.

### 3.6. Parametric Study of $L_C$

The variation of $L_C$ affects the impedance matching of the antenna. The value of $L_C = 1.75$ mm is selected for the final design, as it gives the best matching over most of the band as shown in Figure 6(f).

## 4. FAR-FIELD PATTERNS

The radiation patterns of the proposed antenna are obtained through numerical calculation using the CST® simulator over the whole operating band. The far-field patterns are shown in Figure 7 at 15 GHz, 20 GHz, 25 GHz, 28 GHz, 30 GHz, 40 GHz, 50 GHz, 60 GHz, and 80 GHz, in the two principal planes, $\phi = 0°$ and $\phi = 90°$.

The antenna gain variation over the frequency band of operation is shown in Figure 8, which indicates that the gain ranges from 2.3 dBi to 7.78 dBi at the operating band of the antenna. The antenna radiation and total efficiencies are shown in Figure 9.

The antenna has a maximum radiation efficiency of 97.8% and a total efficiency of 84%.

## 5. PROPOSED QUAD-PORT MIMO SYSTEM

A compact quad-port MIMO antenna system configuration with dimensions $L \times L$ equal to 30 mm $\times$ 30 mm is proposed for efficient MIMO operation. The system is constructed with orthogonal arrangement of the four antennas, such that each antenna is rotated by 90° with respect to its neighbors, as shown in Figure 10. This gives a polarization diversity for the MIMO system. Each antenna can transmit and receive in a particular direction. Figure 11 shows the reflection coefficient at each port, which shows a coincidence for all ports. The coupling between the MIMO antenna elements is an important parameter to study. It indicates how much an antenna is affected by its neighbors. It is desirable for the mutual coupling parameter to be as minimum as possible. The mutual coupling parameters corresponding to the four antennas are shown in Figure 12. From Figure 12, we can see excellent levels for mutual coupling. The mutual coupling for the four antennas can also be assessed through the surface current distribution shown in Figure 13. From the figure, we can see the amount of surface current coupled to the antenna neighbors, which ensures low mutual coupling levels for all antennas. The 3D radiation patterns for the MIMO system at different frequencies are shown in Figure 14.

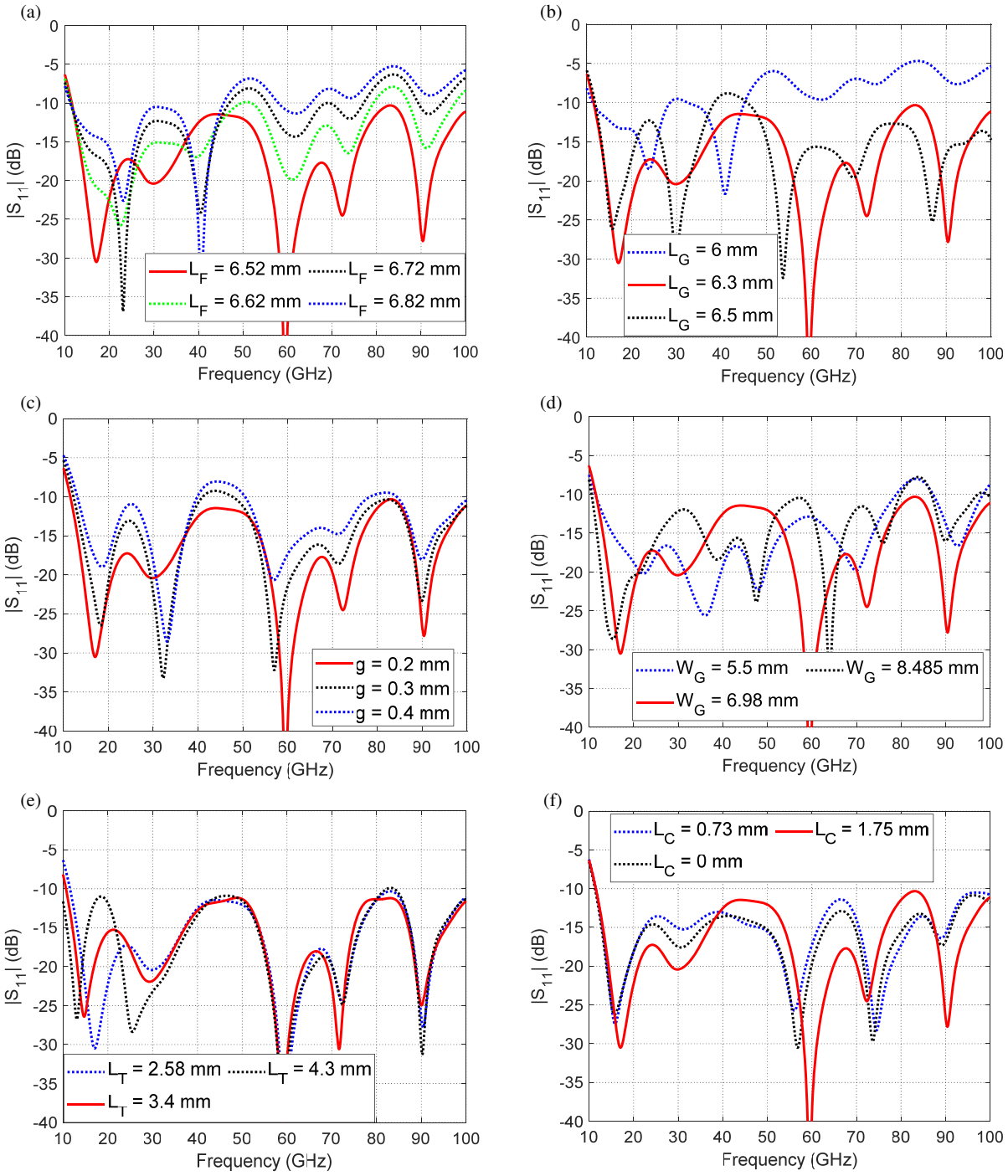


**FIGURE 6**. Parametric study for the proposed antenna.

## 6. MIMO SYSTEM PERFORMANCE

The parameters of the MIMO system, such as ECC and DG, are investigated in this section.

### 6.1. Envelope Correlation Coefficient (ECC)

The value of ECC is preferred to be as low as possible, as it shows the dependence of each antenna radiation on the other antennas' radiation. A lower value of the ECC means low correlation between the antenna elements, higher quality of the signal, lower interference, and higher capacity [21]. The ECC is calculated as follows [12]:

$$\mathrm{ECC} = \frac{\left|S_{11}^{*}S_{12} + S_{21}^{*}S_{22}\right|^{2}}{\left(1 - |S_{11}|^{2} + |S_{21}|^{2}\right)\left(1 - |S_{22}|^{2} + |S_{12}|^{2}\right)} \quad (3)$$

ECC versus frequency is shown in Figure 15. From this figure, it is clear that the worst value of ECC is 0.06, which is a very low value. This means a low correlation coefficient.

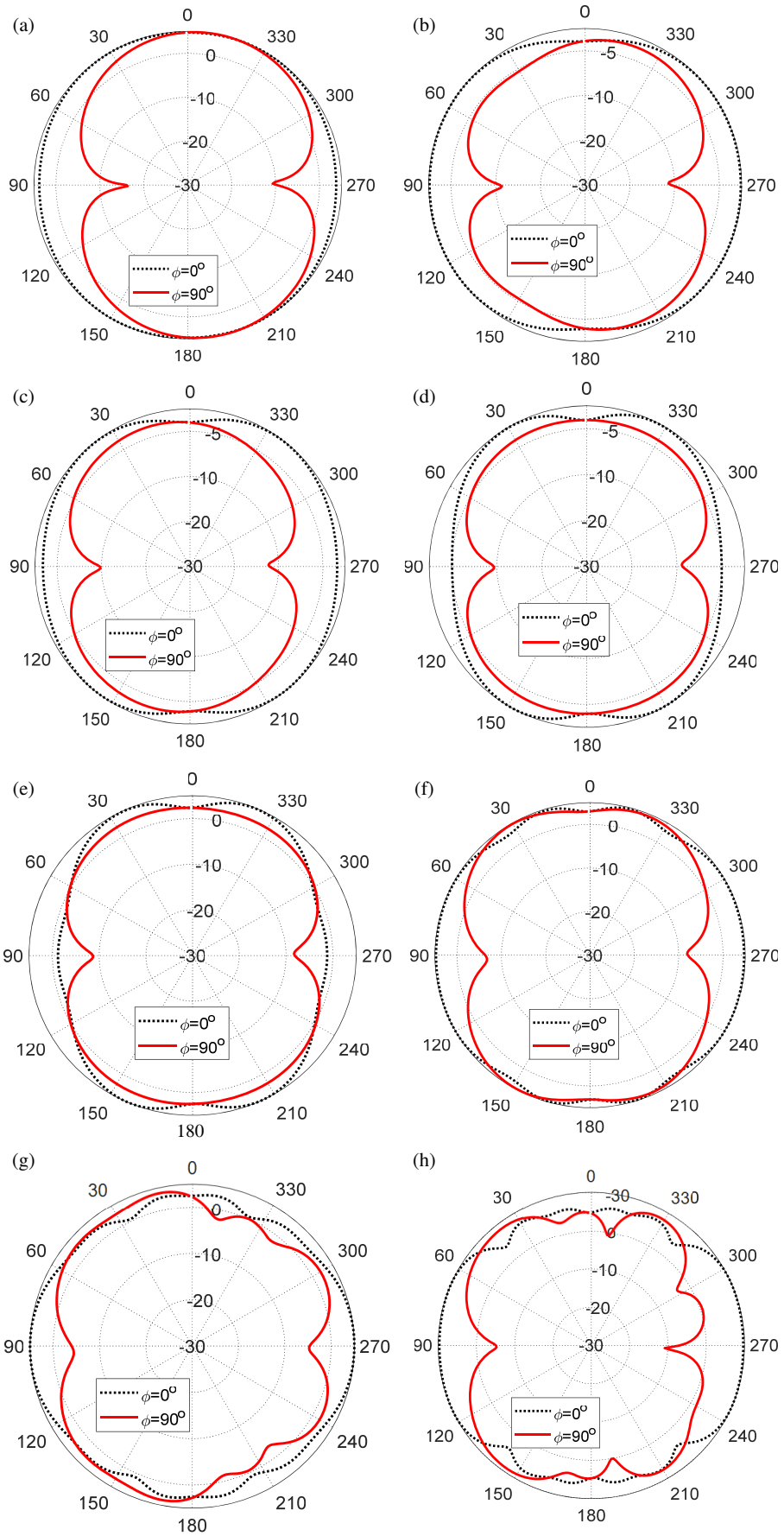


**FIGURE 7**. Radiation patterns of the proposed antenna in the two planes $\phi = 0°$ and $\phi = 90°$, at (a) 15 GHz, (b) 20 GHz, (c) 25 GHz, (d) 28 GHz, (e) 30 GHz, (f) 40 GHz, (g) 50 GHz, and (h) 60 GHz.

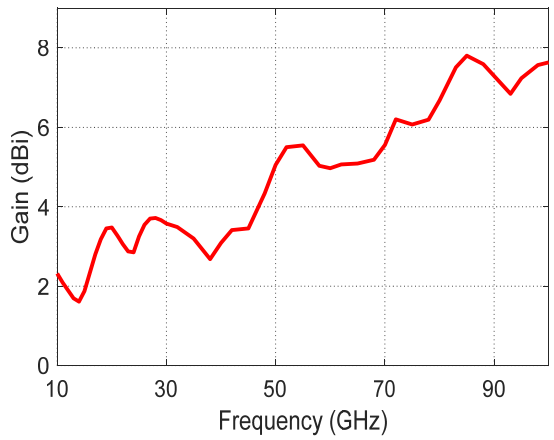


**FIGURE 8**. Gain variation over frequency for the proposed antenna.

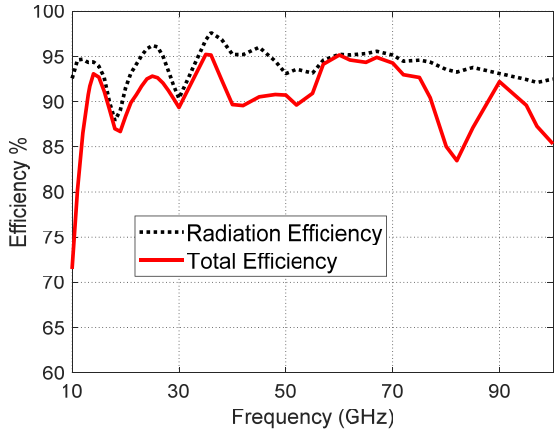


**FIGURE 9**. Efficiency variation over frequency for the proposed antenna.

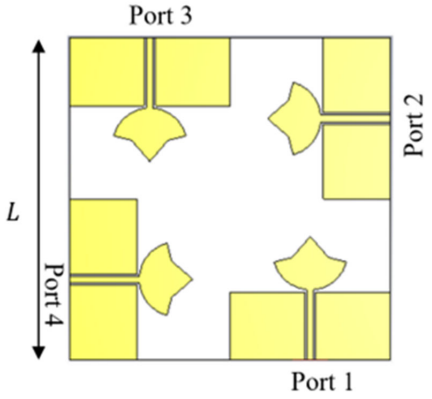


**FIGURE 10**. Quad-port MIMO system.

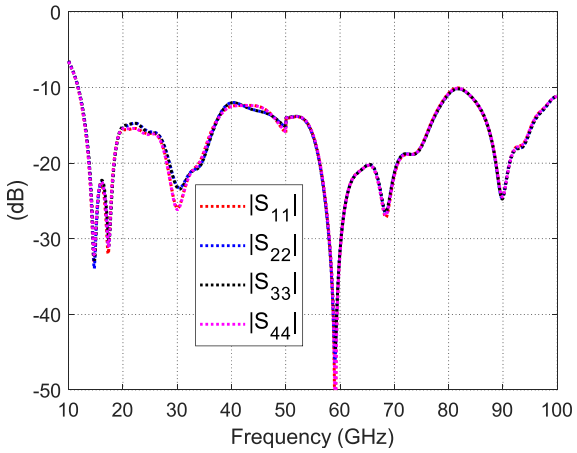


**FIGURE 11**. Reflection coefficients at the four ports.

**TABLE 2**. Comparison for the presented MIMO antenna system and some published MIMO systems.

| Ref. | No of ports | Operating band (GHz) | Gain (dBi) | Size ($\lambda \times \lambda$) | Element spacing (mm) | Isolation (dB) | ECC/DG (dB) |
|---|---|---|---|---|---|---|---|
| [10] | 1 | 1.22–47.5 | 10.3 | $0.16 \times 0.18$ | - | - | - |
| [11] | 2 | 3.28–17.8 | 4.93 | $0.437 \times 0.251$ | 3.38 | $> 20$ | 0.003/9.997 |
| [12] | 4 | 2.4–18 | 5 | $0.4 \times 0.4$ | 15 | 30 | 0.00021/9.9 |
| [15] | 2 | 1.78–30 | 6.6 | $0.21 \times 0.14$ | 10 | $> 22$ | 0.1/NA |
| [16] | 4 | 2.9–40 | 13.5 | $0.56 \times 0.56$ | 10 | $> 17$ | $< 0.04$/NA |
| [17] | 4 | 1.3–40 | 7 | $0.24 \times 0.24$ | 16.9 | $> 22$ | $< 0.03$/NA |
| [22] | 2 | 25.988–26.676 | 5 | $2.363 \times 0.953$ | 8 | $> 30$ | 0.001/NA |
| [23] | 2 | 27–28.16 | 4.8 | $0.972 \times 1.76$ | 4.25 | $> 25$ | 0.01/NA |
| [24] | 2 | 25.5–30 | 5.7 | $2.55 \times 1.27$ | 5.3 | $> 32.3$ | 0.001/NA |
| [25] | 4 | 26–60 | 11.1 | $2.16 \times 2.25$ | 10 | $> 36$ | 0.001/NA |
| [26] | 2 | 34.1–39.7 | 6.7 | $0.68 \times 1.9745$ | 8.33 | $> 65$ | 0.00035/NA |
| [27] | 2 | 25–31.6 | 4.8 | $0.9 \times 1.636$ | 5.82 | 25 | 0.01/9.99 |
| [28] | 4 | 20–40 | 17.6 | $1.73 \times 1.667$ | 9 | $> 20$ | 0.001/9.9 |
| [29] | 4 | 3.1–17.3 | 5.5 | $0.59 \times 0.59$ | 10 | 14.5 | $< 0.1$/NA |
| [30] | 4 | 2.15–20 | 5 | $0.308 \times 0.308$ | 2 | 20 | 0.1/NA |
| [31] | 4 | 2.7–10.6 | 3.5 | $0.54 \times 0.54$ | 7 | 15 | 0.063/NA |
| Presented | 4 | 11.5–100 | 8.37 | $1.15 \times 1.15$ | 8.7 | $> 20$ | 0.06/9.7 |

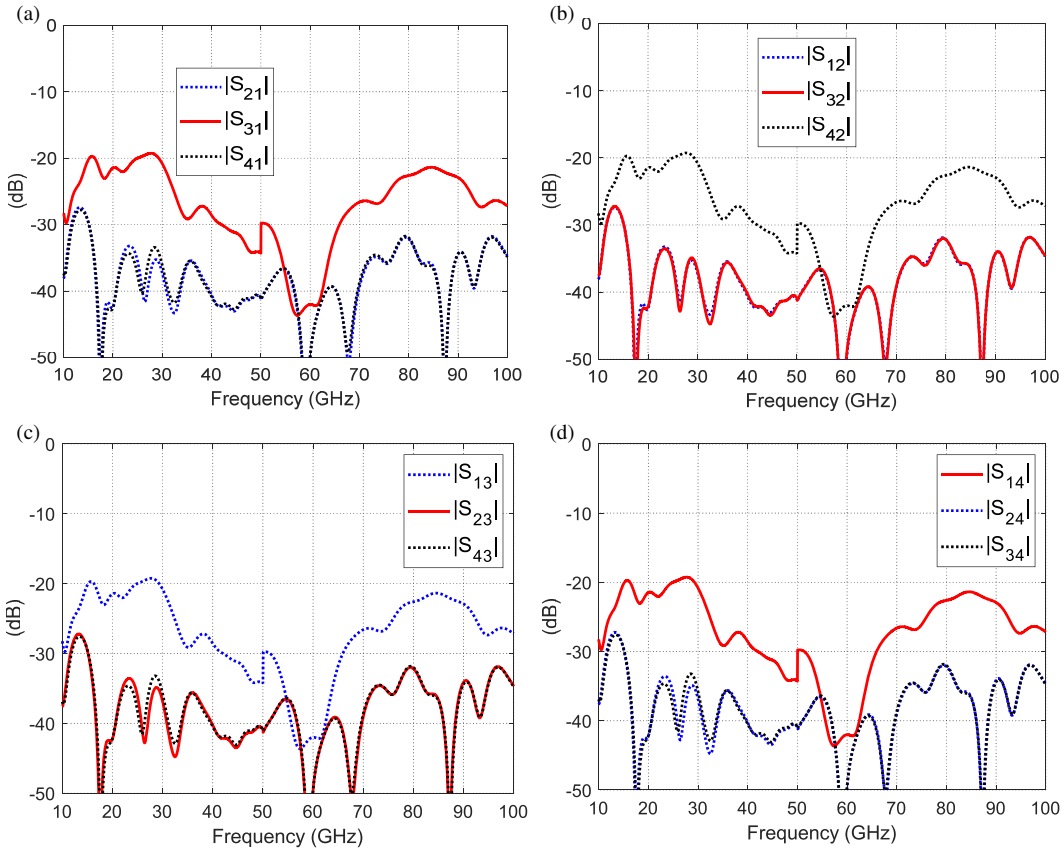


**FIGURE 12**. Mutual coupling between MIMO system elements at (a) port 1, (b) port 2, (c) port 3, (d) port 4.

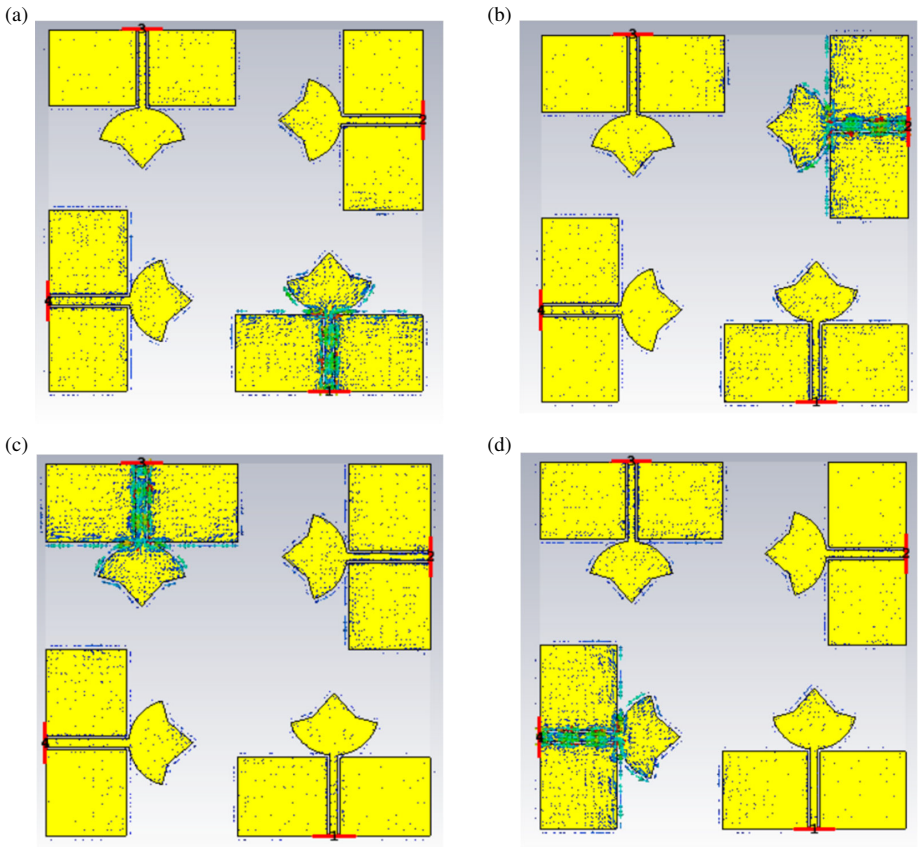


**FIGURE 13**. Coupling between MIMO elements with different antennas working, separately, (a) antenna 1, (b) antenna 2, (c) antenna 3, (d) antenna 4.

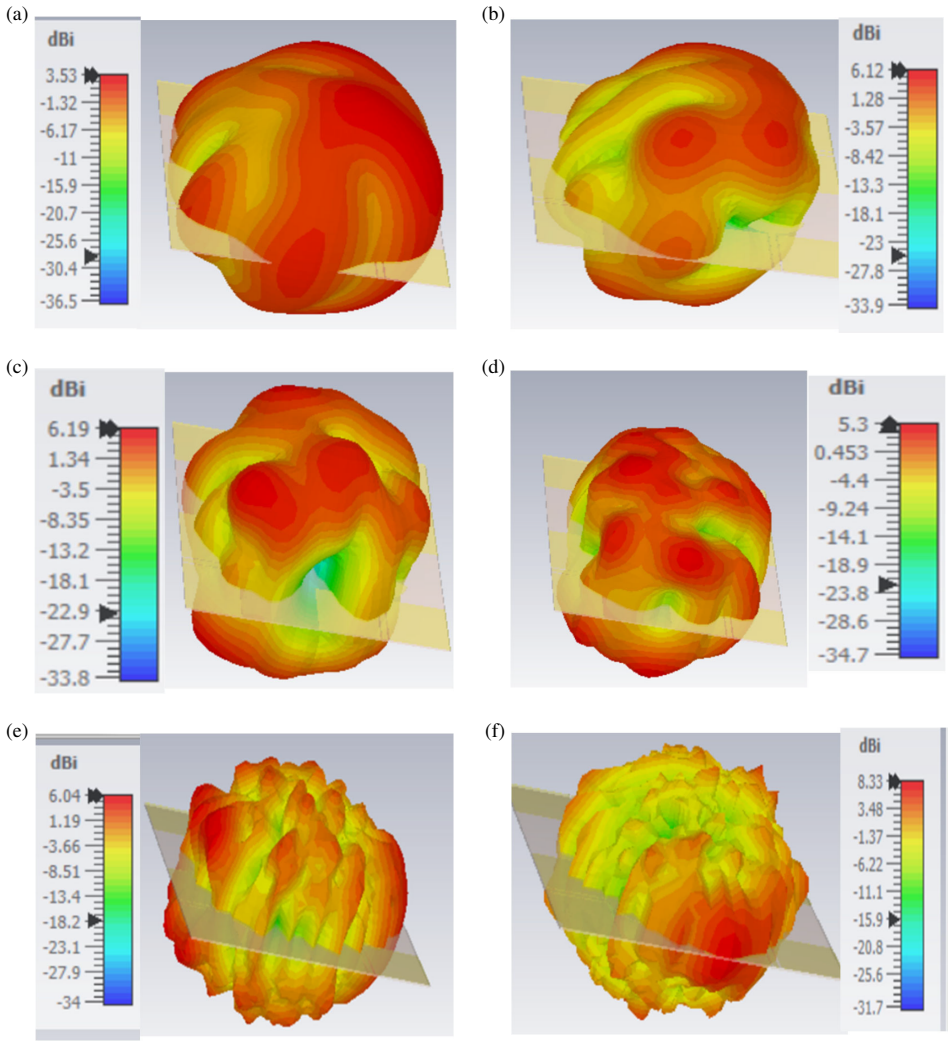


**FIGURE 14**. 3D radiation patterns for the MIMO system at (a) 15 GHz, (b) 20 GHz, (c) 30 GHz, (d) 40 GHz, 60 GHz, and 90 GHz.

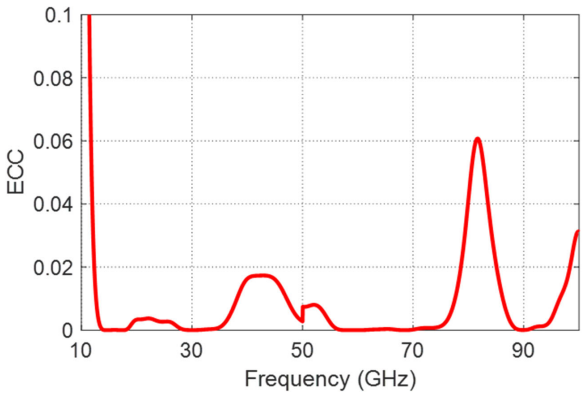


**FIGURE 15**. ECC for the MIMO system.

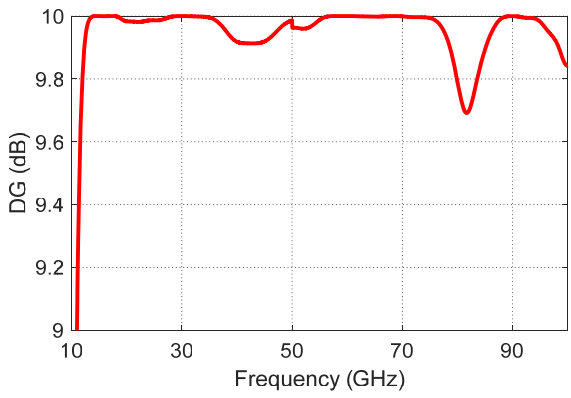


**FIGURE 16**. MIMO system diversity gain.

### 6.2. Diversity Gain (DG)

It refers to the improvement in communication reliability achieved by using multiple independent antennas to transmit and receive signals. A large value for DG is preferred, as it means that the system can combat the fading effects and enhance signal quality, leading to increased coverage and better overall performance. It is calculated as follows [12]:

$$\mathrm{DG} = 10 \times \sqrt{1 - \mathrm{ECC}^2} \tag{4}$$

The DG illustrated in Figure 16 shows an excellent level ranging from 9.7 dB to 10 dB over the whole band.

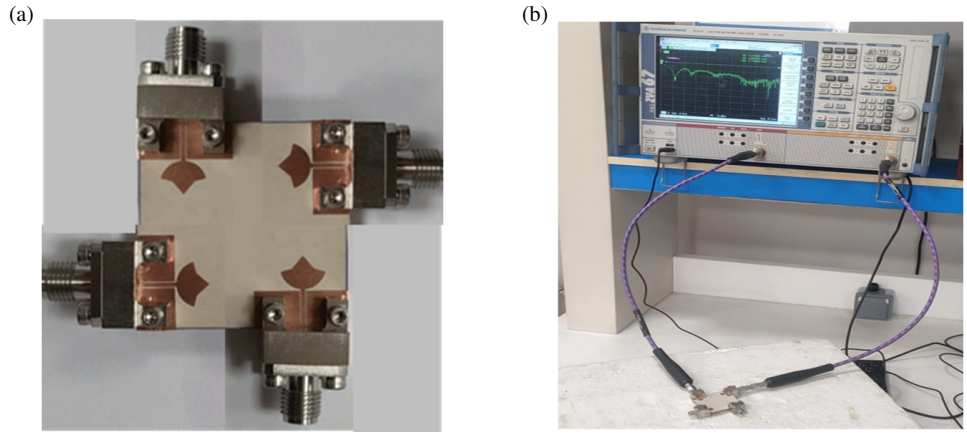


**FIGURE 17**. (a) Fabricated antenna, (b) antenna under test.

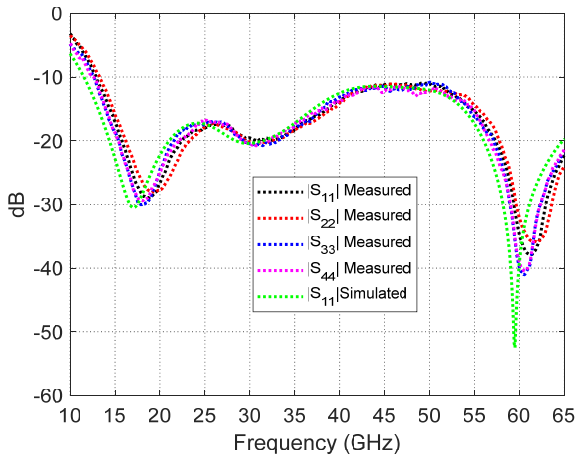


**FIGURE 18**. Comparison between the simulated and measured reflection coefficients of the proposed MIMO system.

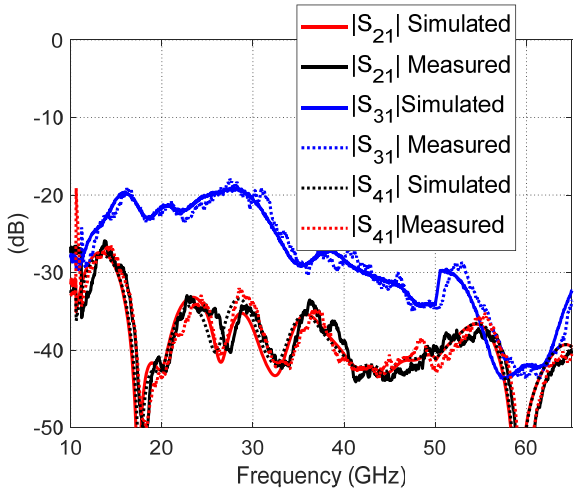


**FIGURE 19**. Comparison between the simulated and measured coupling coefficients of the proposed MIMO system.

## 7. FABRICATION AND MEASUREMENTS

For the verification of the simulation results, the MIMO antenna system is fabricated, and its $S$-parameters are measured. The prototype of the proposed MIMO system is shown in Figure 17(a).

The reflection coefficients of the MIMO system are measured through the vector network analyzer. Figure 17(b) shows the MIMO system under test. The measurements of the reflection coefficient at the four ports are shown in Figure 18. In addition, the measured coupling coefficients corresponding to the first antenna in the MIMO system are shown in Figure 19. A good agreement between the measurements and simulation results is achieved.

## 8. COMPARISON BETWEEN THE PRESENTED MIMO ANTENNA SYSTEM AND THE STATE-OF-THE-ART SYSTEMS

In this section, a comparison between the proposed MIMO antenna system and some published MIMO systems, regarding the operating bandwidth, achieved gain, size, spacing between MIMO elements, isolation, ECC, and DG, is presented. From the comparison in Table 2, it is shown that the presented MIMO system has higher bandwidth than other compared antennas.

## 9. CONCLUSION

A new design for a compact super-wideband antenna was presented. It covers a large portion of X, Ku, K, Ka, V, and W bands. It can be used for the CubeSat communications in Ku and Ka bands. It is also applicable to 5G communications, as it covers the 28 GHz and 38 GHz bands. The single antenna element operating frequency ranges from 11.5 GHz to greater than 100 GHz. The antenna has a maximum gain of 8.7 dBi. The four-port MIMO antenna system is orthogonally organized. The MIMO system has a coupling less than $-20$ dB. The MIMO system achieves a maximum ECC of 0.06 and a DG about 9.7. The MIMO antenna system performance is experimentally verified. A good agreement between measurements and simulation results is reported.

## REFERENCES


[1] Islam, M. T., M. S. Mahmud, M. H. Islam, A. Shahriar, S. S. Islam, M. R. I. Faruque, and A. H. Gulib, "Design of a microstrip patch antenna for the Ku band applications," *Materials Today: Proceedings*, Vol. 42, 1502–1505, 2021.

[2] Saini, A. S., A. Sharma, P. Srivastava, and K. Anjali, "Design of wideband microstrip antenna for X, Ku and K-band applications," in *2021 International Conference on Advance Computing and Innovative Technologies in Engineering (ICACITE)*, 723–725, Greater Noida, India, 2021.

[3] Zahid, M., M. M. Taqdeer, and Y. Amin, "A compact dual-band microstrip patch antenna for C- and X- and Ku-band applications," in *The 8th International Electrical Engineering Conference*, Vol. 46, No. 1, 16, Karachi, Pakistan, 2023.

[4] Chung, M.-A., K.-C. Tseng, and I.-P. Meiy, "Antennas in the internet of vehicles: Application for X band and Ku band in low-earth-orbiting satellites," *Vehicles*, Vol. 5, No. 1, 55–74, 2023.

[5] Chaudhary, A. K. and M. Manohar, "A modified SWB hexagonal fractal spatial diversity antenna with high isolation using meander line approach," *IEEE Access*, Vol. 10, 10 238–10 250, 2022.

[6] Salah, M. M., M. Hossam, H. A. Ragheb, and A. R. Eldamak, "Efficient super-ultra-wideband monopole antenna design for multi-band wireless applications," in *2024 International Telecommunications Conference (ITC-Egypt)*, 531–536, Cairo, Egypt, 2024.

[7] Siahcheshm, A., J. Nourinia, Y. Zehforoosh, and B. Mohammadi, "A compact modified triangular CPW-fed antenna with multioctave bandwidth," *Microwave and Optical Technology Letters*, Vol. 57, No. 1, 69–72, 2015.

[8] Singhal, S. and A. K. Singh, "CPW-fed octagonal super-wideband fractal antenna with defected ground structure," *IET Microwaves, Antennas & Propagation*, Vol. 11, No. 3, 370–377, 2017.

[9] Gaur, S., D. Lodhi, S. Singhal, and M. Salim, "Compact flower shape super wideband antenna for mmWave applications," in *2022 URSI Regional Conference on Radio Science (USRI-RCRS)*, Indore, India, 2022.

[10] Balani, W., M. Sarvagya, A. Samasgikar, T. Ali, and P. Kumar, "Design and analysis of super wideband antenna for microwave applications," *Sensors*, Vol. 21, No. 2, 477, 2021.

[11] Devana, V. N. K. R., N. Radha, P. Sunitha, F. N. Alsunaydih, F. Alsaleem, and K. Alhassoon, "Compact MIMO UWB antenna integration with Ku band for advanced wireless communication applications," *Heliyon*, Vol. 10, No. 5, e27393, 2024.

[12] Elsharkawy, R. R., A. S. A. El-Hameed, and S. M. El-Nady, "Quad-port MIMO filtenna with high isolation employing BPF with high out-of-band rejection," *IEEE Access*, Vol. 10, 3814–3824, 2021.

[13] Sehrai, D. A., M. Abdullah, A. Altaf, S. H. Kiani, F. Muhammad, M. Tufail, M. Irfan, A. Glowacz, and S. Rahman, "A novel high gain wideband MIMO antenna for 5G millimeter wave applications," *Electronics*, Vol. 9, No. 6, 1031, 2020.

[14] Munir, M. E., A. G. A. Harbi, S. H. Kiani, M. Marey, N. O. Parchin, J. Khan, H. Mostafa, J. Iqbal, M. A. Khan, C. H. See, and R. A. Abd-Alhameed, "A new mm-Wave antenna array with wideband characteristics for next generation communication systems," *Electronics*, Vol. 11, No. 10, 1560, 2022.

[15] Hussain, S. A., F. Taher, M. S. Alzaidi, I. Hussain, R. M. Ghoniem, M. F. A. Sree, and A. Lalbakhsh, "Wideband, high-gain, and compact four-port MIMO antenna for future 5G devices operating over Ka-band spectrum," *Applied Sciences*, Vol. 13, No. 7, 4380, 2023.

[16] Yu, C., S. Yang, Y. Chen, W. Wang, L. Zhang, B. Li, and L. Wang, "A super-wideband and high isolation MIMO antenna system using a Windmill-shaped decoupling structure," *IEEE Access*, Vol. 8, 115 767–115 777, 2020.

[17] Kumar, P., S. Urooj, and A. Malibari, "Design and implementation of quad-element super-wideband MIMO antenna for IoT applications," *IEEE Access*, Vol. 8, 226 697–226 704, 2020.

[18] Elabd, R. H. and A. A. Megahed, "Isolation enhancement of a two-orthogonal printed elliptical slot MIMO antenna array with EBG structure for millimeter wave 5G applications," *Discover Applied Sciences*, Vol. 6, No. 5, 222, 2024.

[19] Luan, H., Y. Wang, C. Chen, and W. Chen, "Mutual coupling reduction of closely E/H-coupled MIMO antennas through metasurfaces," in *2019 International Symposium on Antennas and Propagation (ISAP)*, 1–3, Xi'an, China, 2019.

[20] Balanis, C. A., *Antenna Theory: Analysis and Design*, 4th ed., John Wiley & Sons, Hoboken, NJ, USA, 2016.

[21] Varzakas, P., "Average channel capacity for Rayleigh fading spread spectrum MIMO systems," *International Journal of Communication Systems*, Vol. 19, No. 10, 1081–1087, 2006.

[22] Islam, T., F. Alsaleem, F. N. Alsunaydih, and K. Alhassoon, "Mutual coupling reduction in compact MIMO antenna operating on 28 GHz by using novel decoupling structure," *Micromachines*, Vol. 14, No. 11, 2065, 2023.

[23] Awan, W. A., E. M. Ali, M. S. Alzaidi, D. H. Elkamchouchi, F. N. Alsunaydih, F. Alsaleem, and K. Alhassoon, "Enhancing isolation performance of tilted Beam MIMO antenna for short-range millimeter wave applications," *Heliyon*, Vol. 9, No. 9, e19985, 2023.

[24] Ahmad, A., D.-Y. Choi, and S. Ullah, "A compact two elements MIMO antenna for 5G communication," *Scientific Reports*, Vol. 12, No. 1, 3608, 2022.

[25] Tiwari, P., V. Gahlaut, M. Kaushik, A. Shastri, G. Siddiqui, and B. Singh, "A high-frequency planar-configured millimeter-wave MIMO antenna for fifth-generation NR operations," *International Journal of RF and Microwave Computer-Aided Engineering*, Vol. 2023, No. 1, 9533725, 2023.

[26] Elalaouy, O., M. E. Ghzaoui, and J. Foshi, "A high-isolated wideband two-port MIMO antenna for 5G millimeter-wave applications," *Results in Engineering*, Vol. 23, 102466, 2024.

[27] Ravi, K. C. and J. Kumar, "Miniaturized parasitic loaded high-isolation MIMO antenna for 5G applications," *Sensors*, Vol. 22, No. 19, 7283, 2022.

[28] Tiwari, P., V. Gahlaut, U. N. Mishra, A. Shastri, and M. Kaushik, "Polarization diversity configuration of millimeter wave MIMO antenna for Ka-band application in 5G wireless networks," *Journal of Electromagnetic Waves and Applications*, Vol. 38, No. 4, 486–507, 2024.

[29] Kayabasi, A., A. Toktas, E. Yigit, and K. Sabanci, "Triangular quad-port multi-polarized UWB MIMO antenna with enhanced isolation using neutralization ring," *AEU — International Journal of Electronics and Communications*, Vol. 85, 47–53, 2018.

[30] Abd El-Hameed, A. S., M. G. Wahab, N. A. Elshafey, and M. S. Elpeltagy, "Quad-port UWB MIMO antenna based on LPF with vast rejection band," *AEU — International Journal of Electronics and Communications*, Vol. 134, 153712, 2021.

[31] Kiem, N. K., H. N. B. Phuong, and D. N. Chien, "Design of compact $4 \times 4$ UWB-MIMO antenna with WLAN band rejection," *International Journal of Antennas and Propagation*, Vol. 2014, No. 1, 539094, 2014.